Design of a two-bladed counterpart to the three-bladed INNWIND 20 MW offshore reference wind turbine

Fabian Anstock[1,*], Marcel Schütt[1,*], and Vera Schorbach[1]

[1]Hamburg University of Applied Sciences, Berliner Tor 21, 20099 Hamburg, Germany
[*]These authors contributed equally to this work.

Correspondence: Fabian Anstock (fabian.anstock@haw-hamburg.de)

Abstract. It is still an ongoing discussion in the wind field whether a two-bladed or a three-bladed rotor is economically superior for large offshore wind applications. While the inherent question is clear, the answer has to tackle a multitude of challenges. One is the task of establishing an equal three- and two-bladed turbine design to fill the research gap on the engineering side. Due to the notorious difficulties of reaching an entirely equal design, the goal is to remain as similar as possible, always with the premise of reaching a fair comparability. For this purpose, the focus of the paper is on striving for the most similar aerodynamics, including an equal absolute power curve, as well as a most similar blade structure in terms of a comparable fiber composite layer stack and matching ultimate and fatigue material stresses and stability limits. The controller features the same architecture and is equipped with basic load mitigation algorithms. The gains are tuned by utilizing an objective control cost criterion. The generator is adapted to the changed torque and rotation speed, and the tower is adapted to fatigue loads. A complete load and cost comparison and further manufacturing, transportation, installation, and operation and maintenance aspects are outside of the scope herein. In turn, the paper presents a thought-through possibility of achieving a most similar two-bladed turbine based on a three-bladed reference. While this re-design could generally be performed with any detailed three-bladed horizontal-axis wind turbine, the steps are showcased on the three-bladed 20 MW INNWIND reference turbine. The final turbine models, controller, and blade models are made open source with the paper at hand.

1 Introduction

The growth trend of modern wind turbines is driven by the steady urge to reduce the levelized cost of energy (LCoE). In this context, the most widely encountered turbine concept is an upwind-orientated three-bladed variable-speed pitch-controlled machine with a fixed hub (McCoy et al., 2024). Nevertheless, it is important to be aware of alternative turbine concepts, especially concerning technological development, improved adaptations to offshore requirements and larger turbine sizes, to reduce the LCoE further. One example is the concept of two-bladed turbines. Wind energy engineers and scientists have discussed the possible potentials of modern two-bladed offshore wind turbines for decades (Anderson et al. (1984); Hohenemser and Swift (1984); Henderson et al. (1989); Larsen et al. (2007); Aagaard Madsen et al. (2013); Mühle et al. (2016); van Solingen et al. (2016); Schorbach et al. (2017); Civati et al. (2018); Burton et al. (2021); Anstock and Schorbach (2024); et al.).

To elaborate on whether two or three blades are more favorable for future turbine generations, especially with regard to the
25   LCoE, various advantages and disadvantages need to be objectively weighed against each other. For this purpose, a fair and
holistic comparison of two- and three-bladed turbines of the state-of-the-art is mandatory. The main task is to tackle the issue
that "Clear-cut cost comparisons between two and three-bladed machines are notoriously difficult because of the impossibility
of establishing equivalent designs" (Burton et al., 2021, p. 381). The herein favored approach is to take a large standard three-
bladed turbine and transform it into a most similar two-bladed turbine, subsequently named its *"two-blade counterpart"*. The
30   aim is to maintain as much of the original design philosophy as possible with the support of several boundary conditions
to gain a most similar design. It features most similar aerodynamics and an equal energy yield achieved by a ~2% larger
rotor. It includes a similar blade structure with equal relative sandwich material thicknesses and a matching strength, stability,
and fatigue lifetime ensured by analytical and numerical evaluations, as well as an objective controller tuning and added
load mitigation methods. With this, the paper summarises and extends previous works (Anstock et al., 2019; Schütt et al.,
35   2020, 2021; Anstock and Schorbach, 2020, 2021). The publicly available three-bladed INNWIND 20 MW offshore reference
turbine (Chaviaropoulos and Milidis, 2017; Sartori, 2019) is chosen as a basis for the conversion to take account of the ongoing
growth trend. Figure 1 gives a first impression of the final outcome.
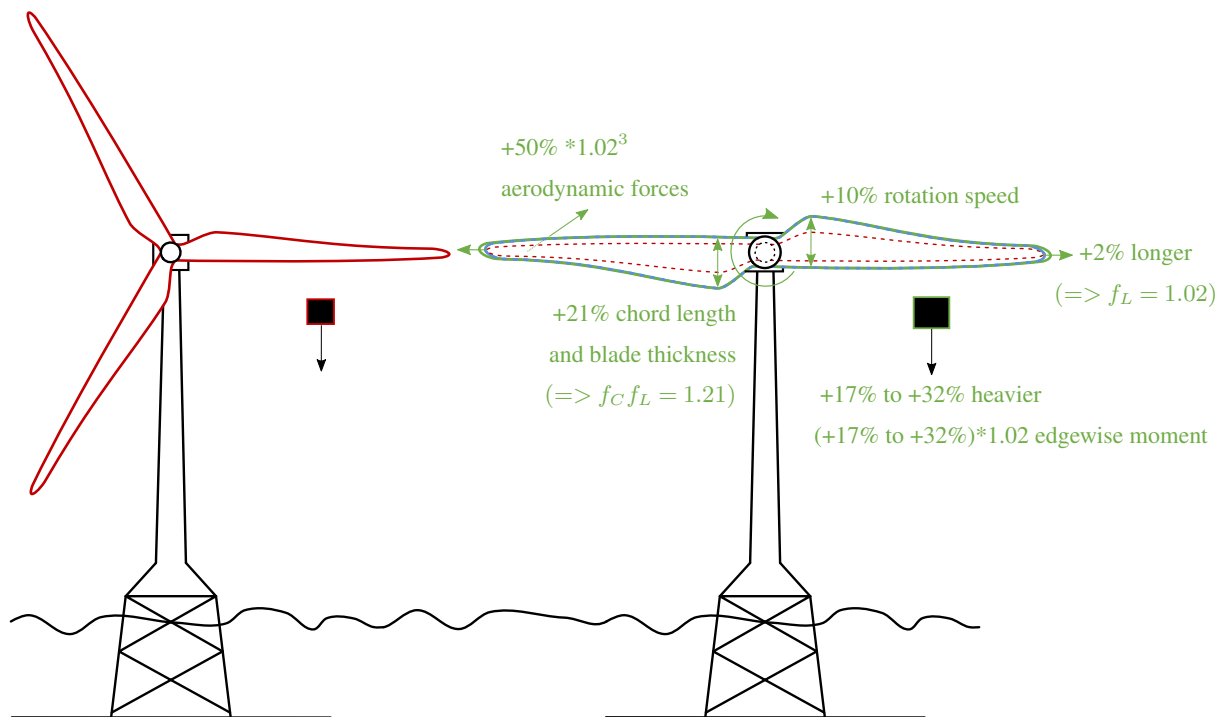
Figure 1. Illustration of the rotor design differences of the three-bladed 20MW INNWIND reference turbine and its two-bladed 20 MW counterpart, including the increase of loads from Jamieson (2018) for +2 % longer blades.

While the re-design process is performed on the basis of the INNWIND 20 MW offshore reference turbine as an example, all the described design steps could also be performed with any other detailed three-bladed turbine to gain its own two-bladed counterpart. The design aspects are ordered as follows:

Section 2) Rotor blade redesign

Section 3) Controller and loads

Section 4) Tower and eigenfrequencies

Section 5) Drive train

The subsequent Section 6 provides an additional blade structure design for a 20 MW two-bladed turbine with a teetering hub, which offers the potential to reduce blade and tower loads and masses. An overall design summary of the 20 MW two-bladed turbines and a critical discussion of the design challenges are given in Section 7. Note that several references have to be made to subsequent sections due to the iterative multidisciplinary loop characteristic of some design aspects.

2 Rotor blade design of the two-bladed counterpart

The blades demand the highest amount of adaptations to develop a two-bladed counterpart of the three-bladed reference turbine, which makes this section the largest. The rotor blades are redesigned for similar aerodynamics and an equal absolute power curve in Section 2.1. The structure is redesigned first for equal strength limits in Section 2.2, second for equal stability limits in Section 2.3, and third for the same fatigue lifetime in Section 2.4.

2.1 Aerodynamic rotor blade surface adaptation

The initial step for creating a most similar two-bladed turbine is an aerodynamic blade surface redesign of the three-bladed reference turbine's blade. The turbine concept and the operating strategy are kept unchanged for a better comparability. Besides that, the two-bladed turbine's blade should utilize the same aerodynamic design concept, in this case, striving for a maximum power coefficient ($C_{P,max}$-design). Equal airfoils and equal relative chord and thickness distributions are applied, meaning that all chord lengths and thicknesses along the blade span are increased by only one single factor f_C. The airfoil positions remain unchanged relative to the blade length. The blade twist is adapted iteratively to achieve the same local angles of attack and thus operate the airfoils with equal lift-to-drag ratios for the corresponding design tip speed by performing quasi-static aerodynamic simulations. By utilizing stiff blades in these simulations, uncertainties of the actual blade stiffness from the subsequent blade structure adaptation can be obviated.

The described aeroelastic redesign can generally be performed for any desired increase of chord length *or* tip speed, while one parameter defines the other. The most popular analytical redesign philosophies are the extremes of increasing either the chord by 50 % (thus $f_C = 1.5$) and maintaining the design tip speed (Larsen et al., 2007; Civati et al., 2018; Mühle et al., 2016) or increasing the tip speed by 22.5 % and maintaining the chord length (Mühle et al., 2016; Burton et al., 2021). Figure 2 (a) shows the power coefficients over the tip speed ratio for a variation of the chord length factors. Every chosen design tip speed specifies the shape and dimensions of the outer blade surface and vice versa. No generally preferable design choice can be made
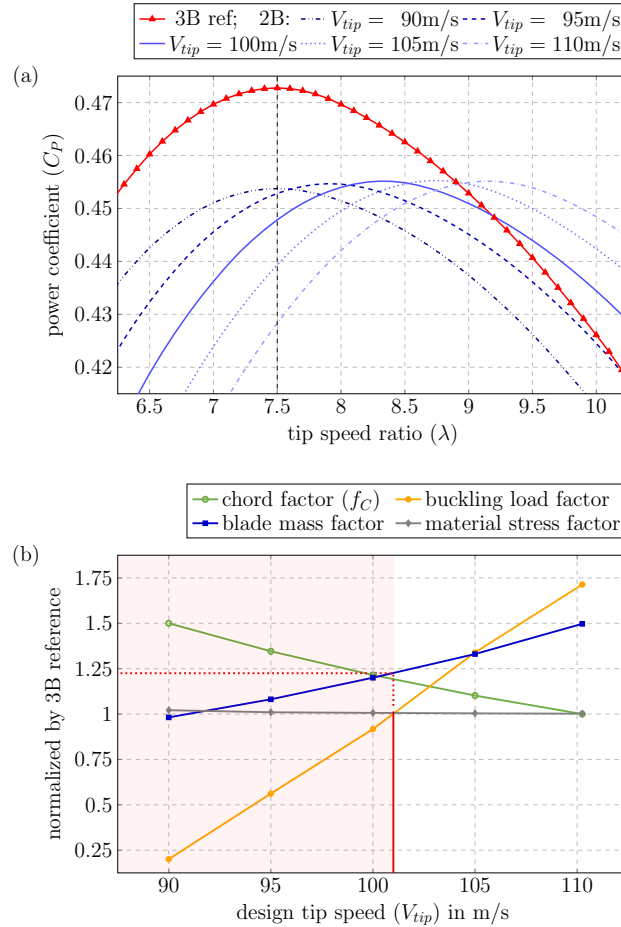
Figure 2. C_P-curves for the three-bladed reference and for most similar two-bladed counterparts with the same rotor diameter and different design tip speeds (a) from Anstock et al. (2019) and corresponding factors for the blades' chord length (Section 2.1), masses and static material stresses (Section 2.2) and buckling factors (Section 2.3) for each tip speed, respectively normalized by the three-bladed reference (b), based on Schütt et al. (2021).

70 since the decision of which combination to use for a (two-bladed) turbine is linked to various advantages and disadvantages (Anstock et al., 2019). As described by Burton et al. (2021), the blade mass m is proportional to the rotation speed Ω, tip speed V_{tip}, and tip speed factor λ and thus anti-proportional to the square root of the chord length factor f_C:

$$m \propto \Omega \propto V_{tip} \propto \lambda \propto f_C^{-1/2} \tag{1}$$

The equation highlights the positive effect of the Huygens-Steiner's Theorem on the second moment of area for wider struc-
75 tures, an important advantage of a two-bladed turbine: a wider blade structure does not need to be +50 % heavier to withstand +50 % higher loads (Larsen et al., 2007), which is also displayed by the blue blade mass line in Figure 2 (b). However, Eq. (1) does not include buckling issues, which drastically increase for wider structures if the composite's core material is not adapted

accordingly, as shown by the yellow buckling factor line in Figure 2 (b). Herein, the final chord length and design tip speed are defined by keeping the structural stability limit of the three-bladed turbine, while aiming to achieve a low mass. The chosen

80   compromise of a 19.5 % longer chord and a 12.2 % higher design tip speed is a result of iterative structural finite element analyses (FEA) with the methods described in (Schütt et al., 2021) and in Section 2.2 and 2.3. This two-bladed aerodynamic redesign is subsequently named 2B101 due to its tip speed of 101 m/s. Figure 2 (b) shows the key factors from the FEA, which are well in line with the analytical Eq. (1). The red area marks the design field where the structural stability limit is lower than the stability limit of the three-bladed reference if the core material thicknesses remain proportionally equal to the original
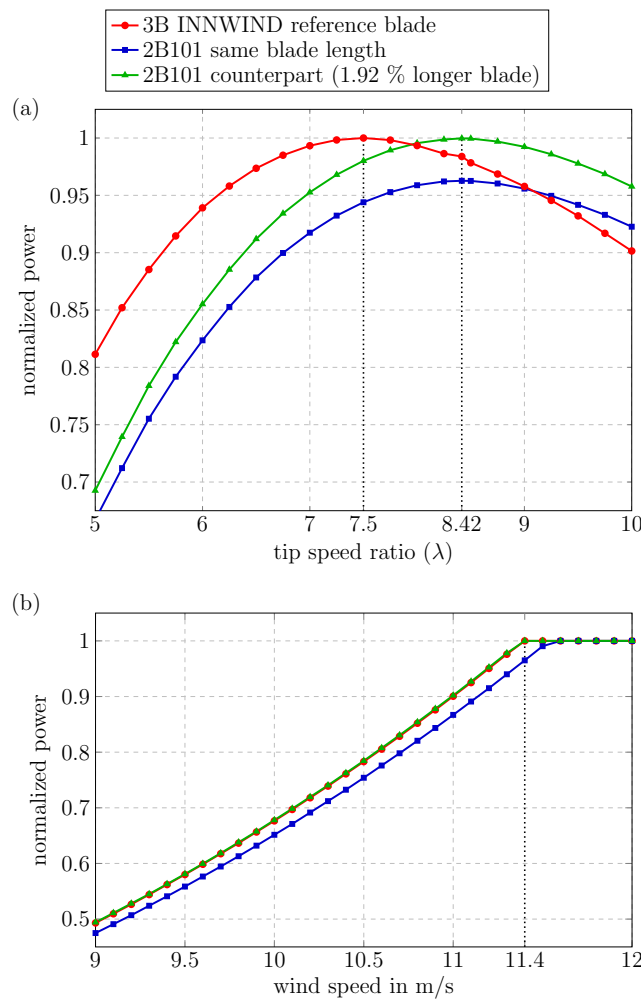
Figure 3. Power curve of the three-bladed reference compared to a two-bladed turbine with same blade length and the two-bladed counterpart: (a) normed power, and (b) normed steady operation power, based on Anstock et al. (2019).

composite layer thicknesses. All tip speeds outside the red area reach the required stability, while the one closest to the area is the lightest and thus most desirable, which caused the method's naming "break-even-point analyses" by Schütt et al. (2021).

The last step of the aerodynamic redesign is to increase the rotor diameter slightly by ∼2 % to counterbalance the lower aerodynamic efficiency and achieve an equal absolute quasi-static power curve. This differs from conventional approaches for comparing two- and three-bladed turbines, which mostly leave the rotor diameter unchanged (Burton et al., 2021; Larsen et al., 2007; Civati et al., 2018; Aagaard Madsen et al., 2013). However, blade tip losses increase for fewer blades, yielding a lower power coefficient C_P for two-bladed turbines if an equal aerodynamic design philosophy is applied (Prandtl, 1923; Burton et al., 2021), as shown in Figure 2 (a). In the case of an unaltered rotor diameter, it would be difficult to compare loads and dynamics directly since they correspond to turbines with different power ratings or rated wind speeds. In contrast, the new approach based on the same absolute quasi-static power curve enables a more straightforward comparison of loads and costs due to an about equal energy production (Anstock et al., 2019). In the case of the 20 MW turbine considered in this work, the aerodynamic power coefficient of the two-bladed turbine with an equal rotor diameter marked in blue in Figure 3 (a), is about 4 % lower, which can be counterbalanced by an increase in blade length of 1.92 %. The result is a two-bladed turbine with exactly the same quasi-static power curve and thus about the same energy yield as the three-blade reference (Anstock et al., 2019) as presented in green in Figure 3 (a) and (b). Note that the peak of the tip speed ratios drifts to the right for the actual flexible blades, becoming more suitable for their rated wind speed of 11.4 m/s that results in ratios of 7.89 and 8.86 for 90 m/s and 101 m/s, respectively.

2.2 Structural rotor blade static strength strength

In terms of a fair structural comparison of two- and three-bladed turbines, the blade structure of the two-bladed counterpart should be adapted to yield at least the same strength and stability limits as the blades of the three-bladed reference turbine.

The static loads are scaled by the "method of progressive structural scaling" from Schütt et al. (2020). The underlying analytical load assumption for equal blade lengths is that the flapwise blade loads of a two-bladed turbine are +50 % higher per blade compared to the three-bladed reference. The edgewise loads, in turn, are assumed to increase proportionally to the blade mass and its first moment of mass about the rotor axis. These assumptions are applied independent of the design tip speeds and chord lengths. Concerning the blade's strength only, a design with +50 % larger chord lengths requires, according to Larsen et al. (2007), the same blade material as the more slender reference blade to withstand +50 % increased edgewise *and* +50 % increased flapwise loads. In that case, the weight and thus gravity-driven edgewise loads are, however, not increased, which enables a further iterative *progressive* reduction of blade material (Schütt et al., 2020). Besides this, the flapwise design loads of the two-bladed counterpart are slightly higher due to the +1.92 % increased blade length for achieving an equal absolute power curve. Based on common scaling laws from Jamieson (2018), the flapwise loads are scaled by the blade length factor $f_L = 1.0192$ to the power of three so that the flapwise loads of the 20 MW two-bladed counterpart are +58.8 % higher compared to the three-bladed reference. The edgewise loads still depend on the blade mass and lever.

The stresses are evaluated by means of FEA. In the work at hand, the program ANSYS® Mechanical APDL (Ansys Parametric Design Language) is utilized. The stresses are determined along the entire blade span at each of the cross-section elements

(e.g. at the spar caps and the shell structure). By adapting the local material thicknesses, the same material stresses can be

120 realized regardless of the utilized chord length or rated tip speed (Schütt et al., 2021). Figure 4 presents the material stresses at different cross-section elements along the blade span. The spar caps at the suction side, the front shell structure at the suction side, and the leading edge reinforcements are shown exemplary, although the analyses were carried out for all elements.
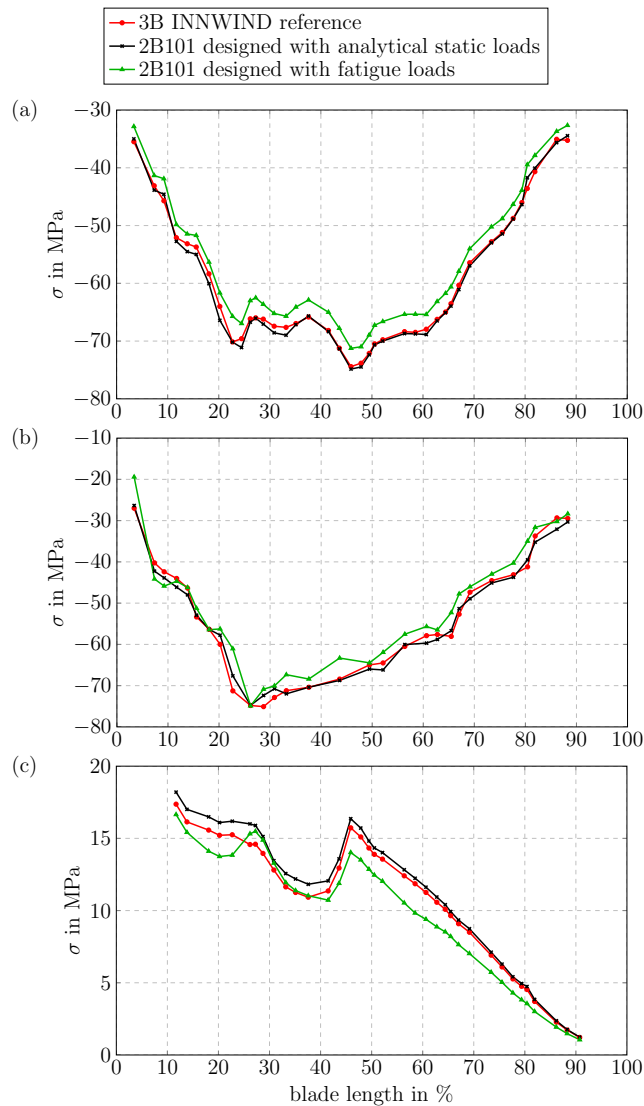
Figure 4. Material stresses at (a) spar caps at the suction side, (b) front shell structure at the suction side, and (c) reinforcement at the leading edge.

A design for the same strength limits basically implies that only the respective ultimate material stress is equal. This would have enabled significant material savings for the new structural designed (two-bladed turbine's) blade since the general design

125   of the reference blade in Figure 4 shows larger regions with much lower strain. Yet, to avoid the biased comparison of a basic three-bladed turbine's blade with an optimized two-bladed turbine's blade, and to account for loading situations that are not considered herein, the material thicknesses have been designed to match the reference material stresses for all structural blade parts along the whole blade (Schütt et al., 2021). The resulting two-bladed turbine's blade is illustrated by the black lines in Figure 4. It can be seen that the stresses are almost equal compared to the three-bladed reference (red lines). The average

130   deviation for the cross-section elements shown here is a maximum of 4.6 % at the leading edge reinforcements in Figure 4 (c). Note that the stresses at the reinforcements are comparatively low. At the suction side spar caps shown in Figure 4 (a) and at the front shell structure at the suction side in Figure 4 (b), the average stress deviation is lower with 1.2 % and 0.7 %, respectively. Therefore, it can be stated that the two-bladed turbine's blade was designed for approximately equal static stresses along the blade, including equal maximum strength limits. Figure 4 also includes a blade (green lines) with the same aerodynamic design

135   but with a structure designed for equal local fatigue stresses along the blade, which is further described in Section 2.4. In the static evaluation, this blade shows mostly less strains, which shows the difficulty of a fair comparability when ensuring both, static strength and fatigue limits, at the same time.

2.3   Structural rotor blade stability design

With the procedure described above, equal material stresses can be realized for any chosen chord length or rated tip speed, as

140   shown by the grey line in Figure 2 (b). This does not account for the structural stability. Due to the utilized boundary condition, established to remain as similar as possible, each local material layer composition thickness is adapted with only one factor. The result is that the ratio between fiber and core material remains unchanged instead of increasing the thickness of the lightweight core of the sandwich structure in the buckling-prone regions. The heavier, thick-walled, quick-rotating, slender-blade designs do consequently have a much higher structural stability than the lighter, thin-walled, slow-rotating, long-chord designs. This

145   leads to a conflict of interest since a lower blade mass is obviously more beneficial for manufacturing costs and gravitation-driven loads. The best compromise between preventing buckling and saving rotor mass is given when the combination of chord length and tip speed is increased just enough to match the buckling stability margin of the three-bladed reference, at least for the chosen boundary condition of the material layer adaptation. To determine the desired combination precisely, a variety of combinations is adapted by Schütt et al. (2021) to possess equal material stresses along the blade, followed by a buckling

150   evaluation, as well in ANSYS® Mechanical APDL under the same loads. The resulting buckling factors are depicted by the yellow line in Figure 2 (b). They yield the trade-off mentioned in Section 2.1 between an increase of chord length by 19.5 % and a faster tip speed of 101 m/s. On this basis, the resulting design features equal strength and stability limits in addition to an equal absolute power curve.

The buckling shape of the three-bladed reference blade is shown in Figure 5 (a) with a buckling load factor of 1.162. The

155   maximum deformation happens on the spar caps at the suction side. The two-bladed design previously shown by the black lines in Figure 4 achieves with 1.158 approximately the same buckling load factor as the reference, visualized in Figure 5 (b). It can be seen that the maximum deformation occurs at the front shell structure at the suction side. This happens due to the changes made to the wall thicknesses as part of the "progressive structural scaling" for equal material stresses in Section 2.2. After

including material adaptions from the following fatigue damage analyses, the buckling load factor of 1.156 in Figure 5 (c) is
160 again very similar.
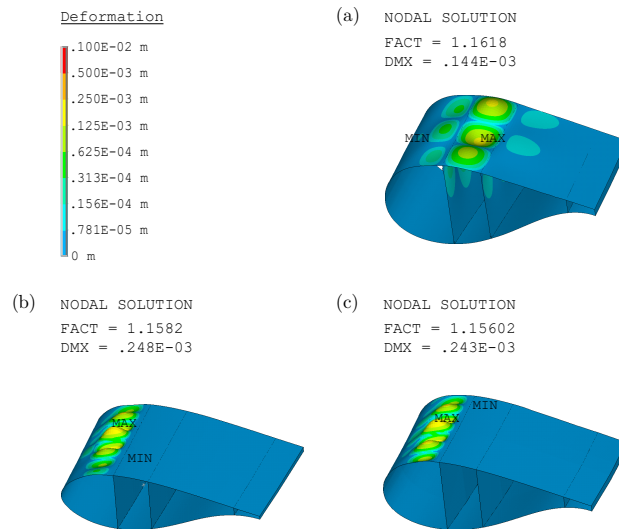
Figure 5. Buckling shape of (a) the three-bladed reference turbine's blade, (b) the two-bladed turbine's blade designed for equal static strength and stability limits based on analytical loads, and (c) the two-bladed turbine's blade after the subsequent fatigue design.

2.4 Rotor blade fatigue design

The third structural aspect to be considered is achieving equivalent fatigue limits through an additional material adaption. In contrast to the previous blade redesign, where the loads were based on analytical equations, the fatigue calculation required load time series from numerical aero-servo-elastic simulations. In the work at hand, the software DNV® Bladed is utilized

165 together with an objectively-tuned, most-similar baseline controller, which is further described in Section 3. The model and the controller can be found in the Github repository listed in the "code and data availability" section below .The evaluated fatigue time series are taken from the design load case (DLC) 1.2 of the guideline IEC-61400-3.2 with the environmental parameters from the reference turbine (Chaviaropoulos and Milidis, 2017). The fatigue damage calculations have been performed with the software BECAS from DTU (Blasques and Stolpe, 2012). The results of the fatigue analyses are presented in Figure 6. The

170 color scheme and the exemplary shown cross-section elements are the same as before.

It has to be emphasized that a design for an equal fatigue live time actually only implies that just the maximum fatigue damage is similar for the two-bladed turbine. This does actually apply to both two-bladed turbine blade designs (black and green lines). The maximum fatigue damage can be seen in Figure 6 (b) at 25 % blade length, which happens to be very similar for all turbines. Yet, only the blade designed for the same fatigue limits along the blade by re-adapting the local material

175 thicknesses (green lines) features similar fatigue damage values over the whole structure. The highest difference of fatigue

damage and, thus, the largest material adaptation occurs in the leading edge reinforcement, shown in Figure 6 (c).
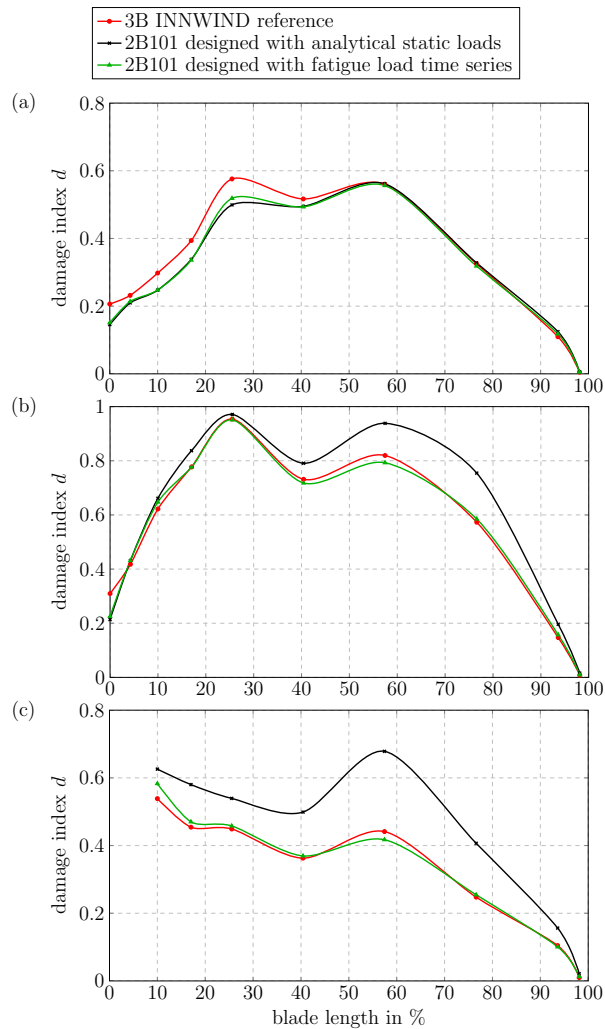
Figure 6. Fatigue lifetime damage at (a) spar caps at the suction side, (b) front shell structure at the suction side, and (c) reinforcement at the leading edge.

Note that the blade fatigue calculations are performed with load time series taken from simulations without active tower dampers, which are closely connected to the utilized tower and foundation design. Thus, the blade fatigue design is independent of the respective performance of the added control features and the tower eigenfrequency issues described in Section 3 and 4.

180 Table 1 summarizes the masses of the redesigned blades compared to the reference. The blade mass of the three-bladed reference is 117.9 t. The two-bladed turbine's blade, designed with analytical loads for equal static strength and stability, weighs 155.2 t. This corresponds to a mass reduction of 12.2 % if all blades are accumulated. The subsequent fatigue design increases

Table 1. Blade masses of (a) the three-bladed reference blade, (b) the two-bladed turbine's blade scaled for equal static strength and stability limits for an analytical load difference, and (c) the same blade after a subsequent fatigue design with loads from DLC 1.2.

blade name	blade weight	$\sum$ total blade mass reduction
(a) 3B reference blade	117.9 t	–
(b) 2B101 equal static stresses (analytical scaled loads)	155.2 t	-12.2 %
(c) 2B101 equal fatigue damages (loads out of DNV® Bladed)	164.4 t	-7.0 %

the blade mass to 164.4 t and lowers the mass reduction to 7.0 % compared to the three-bladed reference. Its final weight is partly caused by the attempt to ensure a conservative comparability: the blade is designed to be equally resistant or superior regarding static stresses *and* fatigue damage values along the whole blade structure, compared to the three-bladed reference. It is a task impossible to achieve without over-designing the overall structure. Hence, the fatigue-driven blade design possesses lower than necessary static stresses, as visible in Figure 4. Furthermore, one could argue that a blade design is even sufficient if the maximal strength and fatigue material limits are not exceeded, while equally lower limits in the non-maximum-loaded areas are unnecessary (see Figure 4 and 6, which do not display flat lines on the level of the respective maxima). However, this would demand throughout-objective optimal-designed blades for both, the two-bladed and the three-bladed turbines, which constitutes an enormous engineering challenge.

Consequently, the resulting designs feature either equal *fatigue* limits along the blade and equal stability limits but over-engineered static strength (Table 1 (c)) or equal *static* strength along the blade and equal stability and fatigue limits (Table 1 (b)). If only the same blade fatigue limit should be maintained, the blade structure design for the static stresses is equally applicable and promoted for further analyses.

3 Controller and loads

The controller of the three-bladed 20 MW offshore reference turbine is given by the publicly available "Basic DTU Wind Energy Controller" from Hansen and Henriksen (2013). It is the baseline controller for the 20 MW two-bladed counterpart. In general, a (re-)tuning of the controller is elementary when re-designing a three-bladed turbine into a two-bladed one. This is mainly due to the fact that a two-bladed turbine possesses another rotor inertia and has, thus, another delayed response to an equal pitch action. To achieve an adequate response, the proportional and integral (PI)-gains of the pitch controller should be tuned objectively. For this purpose, Anstock and Schorbach (2020) have established a control cost criterion (CCC), which approximates the influence of the turbine controller on the dynamic loads and associated component costs. For the sake

of consistency, the PI-gains of the three-bladed turbine are re-tuned likewise, which mainly resulted in a lower I-gain. The
respective values are presented in Anstock and Schorbach (2020).

Unfortunately, the tower loads of the 20 MW two-bladed turbine are significantly higher. This is due to an inconveniently
placed tower eigenfrequency interacting with the blade-passing 2P-frequency, which is a result of a tower being designed for
a three-bladed turbine, as described in Section 4. Therefore, three controller extensions have been added to mitigate the tower
loads. These are a speed exclusion zone, which ensures a transition of the respective blade-passing frequency through the
critical tower frequency as quickly as possible in below-rated conditions, as well as a pitch-driven fore-aft and a generator-
driven side-to-side damper (Anstock and Schorbach, 2021). Note that such control features also reduce the loads of the three-
bladed reference turbine. With regard to a fair comparison, these features are consequently applied to the three-bladed reference
and its two-bladed counterpart and respectively tuned by the CCC. Thus, the controller is adapted and developed further to suit
the needs of both, the two- and three-bladed turbine, in an equal manner.
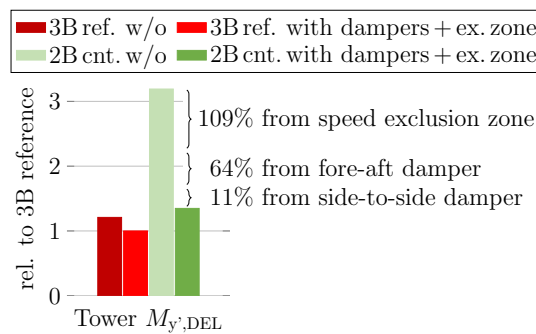
Figure 7. Influence of the added control features on the tower fatigue loads from DLC 1.2 of the three-bladed reference and its two-bladed
counterpart, according to Anstock and Schorbach (2021).

The influence of the controller on the tower fatigue loads for numerical simulations in DNV®'s Bladed is visualized in
Figure 7. Compared are the damage equivalent loads (DEL) of the fatigue load case DLC 1.2, used as well in Section 2.4. With
the added control features, the tower base bending fatigue moment is reduced from +219 % down to only +35 %, relative to the
three-bladed reference that is also equipped with these control features. This is a relative load reduction of ∼184 %, which is
a combination of ∼109 % from the speed exclusion zone, ∼64 % from the fore-aft damper, and ∼11 % from the side-to-side
damper (Anstock and Schorbach, 2021).

Table 2 provides an overview of the blade loads. The analytical assumption during the static structural redesign in section 2.2
is that the flapwise ultimate load of a two-bladed turbine's blade is +50 % higher compared to a three-bladed reference with
an equal rotor diameter and +58.8 % higher for the two-bladed counterpart with a 1.92 % larger rotor. The edgewise loads are
scaled by the blade's first moment of mass about the rotor axis. As mentioned, the controllers have been tuned with the control
cost criterion. It rates the large decrease in tower loads higher than the comparably smaller increase in flapwise blade loads
from +42.5 % up to +59.5 % (see Table 2). The latter matches the load factor of the analytical quasi-static load assumption
well. The increase is mainly caused by the pitch-driven tower fore-aft damper, which is essential to reduce the main tower

Table 2. Comparison of the two-bladed turbine's analytical and fatigue blade loads relative to the three-bladed INNWIND reference.

	flapwise root bending M_y	edgewise root bending M_x
analytically scaled quasi-static loads	+58.8 %	+37.1 %
fatigue loads w/o dampers+ex. zone	+42.5 %	+42.4 %
fatigue loads with dampers+ex. zone	+59.5 %	+43.8 %

fatigue loads. The generator-driven tower side-to-side damper and the speed exclusion zone have a negligible influence on the blade loads. With a more suitable tower eigenfrequency, explicitly placed for a two-bladed turbine and thus not shortly beneath the 2P-frequency, these damping actions might become obsolete.

4 Tower description and eigenfrequency issue

Bearing in mind a fair comparability, the general tower and foundation design are equal for all turbines. This consequently results in similar tower eigenfrequencies. In an ideal case, the original tower design harmonizes well with the respective blade-passing frequencies, which are the trice-per-revolution (3P)-excitation for the three-bladed turbine and the twice-per-revolution (2P)-excitation for the two-bladed turbine. Unfortunately, this is not the case herein. The tower-eigenfrequency is placed, by purpose (Chaviaropoulos and Milidis, 2017), in the middle region between 1P and 3P at rated conditions, which is a typical so-called soft-stiff tower design. It only interferes with the three-bladed turbine's main excitation 3P-frequency at low wind speeds with low occurrences and low aerodynamic loads, as displayed in Figure 8, which renders it a very reasonable design for the reference turbine. For this 20 MW two-bladed turbine, the first tower eigenfrequency is placed just 34 % beneath its main excitation: its rated 2P-frequency. The 2P-frequency is thus close to the tower eigenfrequency in a majority of the below-rated and at-rated conditions. It is this fact that leads to significantly higher tower loads, despite the implemented speed-exclusion zone and active tower dampers described in Section 3.

For the sake of consistency with the 20 MW INNWIND reference turbine, the jacket foundation and the tower are not changed in the aero-serve-elastic two-bladed turbines' Bladed models. Nonetheless, the tower base fatigue bending loads in the worst load direction of the two-bladed counterpart are 35 % higher than the respective fatigue loads of the three-bladed reference turbine (see Figure 7). This is acknowledged in the costs by theoretically increasing the tower and jacket pile wall thicknesses by the given 35%. Thickening the tower walls while leaving the tower section unchanged results in a proportional increase in the tower's cross-sectional area and its second moment of area. Consequently, the tower mass and stiffness are both increased by the same factor as the loads. This would lead to a similar stiffness-to-strength ratio as the reference tower, and thus, according to Blevins (2015), to a similar Rayleigh's Quotient and, therefore, to a similar tower eigenfrequency. A minor change is unavoidable because the mass at the tower top is not affected by this scaling.
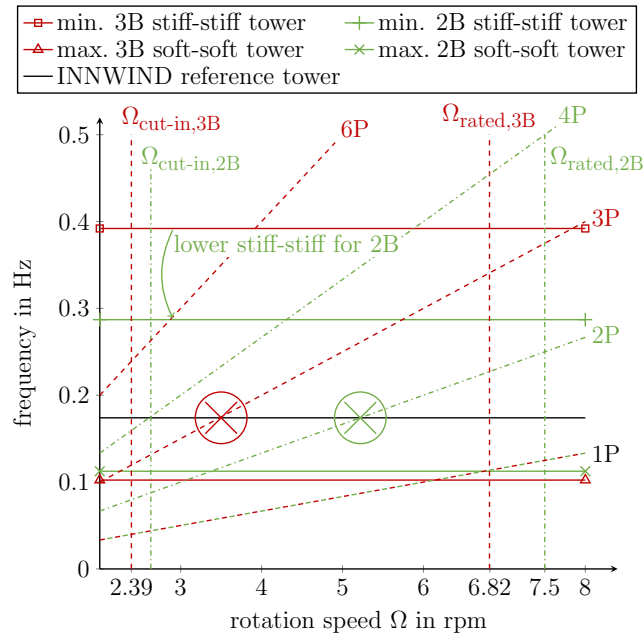
Figure 8. Campbell diagram with the natural frequencies of the INNWIND reference tower and general stiff-stiff and soft-stiff tower designs with 10 % distance margins for two- and three-bladed turbines, together with the periodic 1P, 2P, 3P, 4P, and 6P excitation frequencies.

While a slightly lower or a *much* higher tower eigenfrequency would be favorable, a respective change of the tower diameter would cause an even higher usage of material if the structural stability limit must not be reduced. In general, material could be saved by increasing the tower diameter and the wall thickness proportionally, which would still ensure the same strength and
255 stability limits. However, this would increase the eigenfrequency of the tower slightly and worsen the dynamic interaction. It should thus only be applied if the first tower frequency is far below or already above the twice-per-revolution (2P) frequency, which is not the case herein, as shown in Figure 8. Further, it should be noted that it is uncertain to the authors whether the tower design is driven by buckling, by static strength, by the clearance to bent blades, by ensuring a sufficient distance between the tower eigenfrequency and the 1P- and 3P-frequencies or by fatigue loads. Only the latter, the fatigue tower loads, are
260 increased for the two-bladed turbine but taken herein as the only design driver. The tower mass assumption of the 20 MW two-bladed counterpart is thus rather conservative. With a deeper knowledge of the actual design driver, the tower could have been redesigned less conservatively and more conveniently for the two-bladed turbine's frequency margin, resulting in a valuable improvement in the turbine's dynamics.

It should also be mentioned that a monopile is a more common offshore foundation type than a jacket (McCoy et al., 2024)
265 and that the tower and monopile diameters of very large turbines might be constrained by manufacturing size limits. For a similar water depth of 50 m, such a monopile design could thus be very close to the 1P-frequencies, as mentioned in the decision against a monopile while designing the INNWIND reference turbine by Chaviaropoulos and Milidis (2017). For a

two-bladed turbine, this might, however, have been the better choice. It would also have been more equally suitable for two- and three-bladed turbines, likewise, as observable in the Campbell plot of Figure 8.

5 Drive train conversion

The original drive train of the INNWIND 20 MW offshore reference turbine is equipped with a gearbox and a generator (Chaviaropoulos and Milidis, 2017). Since the two-bladed counterpart rotates faster, its drive train has to be adapted for the higher speed. To accomplish the scaling for the higher speed, a detailed specified drive train is necessary. A direct drive is the herein-favored concept to reduce the re-design options. Otherwise, it is unclear whether to utilize the increase in speed and reduction of torque for mass and cost savings in the generator or the gearbox. Therefore, the detailed and publicly available direct drive of the 15 MW IEA reference wind turbine (Gaertner et al., 2020) has instead been used as a basis. It has been upscaled, first to the correct rated power of 20 MW, and then to the given three-bladed turbine's rated rotor speed of 6.8 rpm, using the scaling laws of Shrestha et al. (2009).

Table 3. Drive train properties as outcome of the drive train conversion based on the 15 MW IEA reference turbine (Gaertner et al., 2020).

	15 MW three-bladed IEA reference	20 MW three-bladed INNWIND reference	20 MW two-bladed counterpart
Rated rotor speed	7.55 rpm	6.82 rpm	7.49 rpm
Generator mass	372 t	524 t	484 t
Generator rotational inertia	$3.17 \cdot 10^6$ kgm^2	$6.14 \cdot 10^6$ kgm^2	$5.29 \cdot 10^6$ kgm^2
Nacelle mass	631 t	1098 t	1050 t
Nacelle inertia (yaw axis)	$18.6 \cdot 10^6$ kgm^2	$36.1 \cdot 10^6$ kgm^2	$35.2 \cdot 10^6$ kgm^2

To avoid a potential dynamical inconsistency with the original 20 MW INNWIND reference turbine, specifically the first fore-aft and side-to-side tower eigenfrequencies, the nacelle's mass and inertia are left unchanged. The original net generator mass of the 15 MW IEA reference wind turbine (Gaertner et al., 2020) amounts to 371.6 t, which makes up 58.9 % of the nacelle mass. Thus, 41.1 % of the nacelle mass is attributed to the yaw drives, the yaw bearing, the main shaft and bearings, the mainframe, and other nacelle parts. For the INNWIND 20 MW reference wind turbine, the net mass of the up-scaled direct drive generator is 523.9 t, which accounts for only 47.7 % of the nacelle mass. This implies a conservative assumption for the other nacelle component masses (yaw drives, etc.). For the +12 % faster rotation speed of the two-bladed counterpart with 7.5 rpm at rated conditions, the utilization of the direct drive scaling laws from Shrestha et al. (2009) results in a 7.7 % reduction of the net generator mass from 523.9 t to 483.8 t. This changes the nacelle mass moments of inertia only slightly. Assuming that the mass of the other nacelle components (yaw drives, etc.) remains unchanged for the two- and three-bladed turbines, it

results in a nacelle mass of 1050.2 t. Accordingly, the two-bladed counterpart's nacelle mass is reduced by 4.35 %. In line with
this and the reduced rotor weight from Section 2, the first tower eigenfrequency unfortunately increased slightly from 0.165 Hz
up to 0.168 Hz for the two-bladed turbine. Table 3 summarizes the results of the drive train conversion.

6   Extending the 20 MW two-bladed counterpart with a teetering hub

The described design of the 20 MW two-bladed counterpart with a fixed hub has led only to small material savings in the rotor
and a significant increase in tower mass due to higher tower loads caused by its unsuitable eigenfrequency. However, a majority
of the two-bladed turbines developed or built to date have additional structural load reduction concepts, with a flexible hub
joint being one of them (Schorbach, 2016). Two-bladed turbines possess the unique ability to apply a teetering hinge in the
rotor hub to balance load differences from both rotor blades (Anderson et al., 1984; Hohenemser and Swift, 1984; Henderson
et al., 1989). But in turn, the design of a teetering hinge is challenging, especially concerning a teeter break, which is necessary
to stop teetering when required, e.g., during shut-down or stand-still of the turbine. Furthermore, teeter end impacts, if present,
do drastically increase the hub loads. Yet, more recent investigations have shown that the harshest teeter extreme loads can be
avoided with a suitable design (Schorbach et al., 2017). Further investigations indicate that the teetering movement is better
dampened and thus less challenging for newer and larger turbines (Anstock and Schorbach, 2024), making teetering worth to
be a reconsidered solution.

Therefore, the presented two-bladed counterpart is extended with a teeter-hub model in DNV®'s Bladed. The model features
a free teeter angle up to 5° and a pitch-teeter coupling via the controller with a coupling coefficient of 2 up from 3° of teeter
angle and a pitch-teeter-velocity coupling coefficient of 3 triggered by an extreme teeter velocity. The gains of the control
features from Section 3 are again re-adapted with the control cost criterion. The aerodynamic blade surface is taken from the
two-bladed fixed-hub turbine, presented in Section 2.1. Utilizing the structural blade redesign steps, described in Section 2.4,
analogously with the teetering turbine's load time series enables another perspective on the 20 MW two-bladed turbine's loads
and masses: The teeter-hub is able to reduce the tower fatigue as well as the blade flapwise fatigue and extreme loads vastly.
The tower base fatigue loading is just +1.3 % instead of +34.8 % (see Section 3) above the load of the three-bladed reference.
Consequently, the tower mass increases only slightly by +1.3 %. This corresponds to a mass reduction of -25 %, which is more
than 450 t.

Looking at the rotor blades, the flapwise root bending fatigue moment is +12.6 % instead of +59.5 % above the loads of the
three-bladed reference (see Table 2). The result is a much lighter blade of 138.3 t instead of 164.4 t. Overall, the results show
that a teetering hinge offers enormous benefits in blade and tower loads.

7   Summary

In the previous sections, the design procedure of a most similar two-bladed counterpart to a three-bladed reference turbine was
described in general and performed based on the 20 MW INNWIND offshore reference wind turbine. This included the blade

design in terms of the aerodynamic surface as well as structural aspects such as static maximum material stresses, buckling, and fatigue stresses in Section 2. The DTU baseline controller has been extended with a speed exclusion zone and active fore-aft and side-to-side dampers in Section 3 to compensate for higher tower loads since the tower eigenfrequency does not harmonize well with the 2P excitations. Although these features lead to an enormous reduction in tower loads, they do not reach the level of the three-bladed reference equipped with the same active load mitigation control features. Therefore, the wall thicknesses of the tower are increased in Section 4 to ensure the same tower material stresses. The drive train was converted from the original gearbox and generator concept to a direct drive in Section 5 in order to facilitate a drive train scaling for a faster rotation speed. After completing the design of the 20 MW two-bladed counterpart, the same procedure was used to create a 20 MW two-bladed turbine with a teetering hub in Section 6. The latter is more favorable in terms of most loads and thus allows to reduce weight on the blades and the tower considerably.

Throughout the complete redesign process, the focus has always been on the fair comparability of two- and three-bladed turbines. When in doubt, the conversion has been made to the favor of the three-bladed turbine to remain conservative. This might also be the most vulnerable aspect of the proposed re-design methodology. Future two-bladed research could address the following points:

1. The blades of two- and three-bladed turbines possess very different chord lengths for similar tip speeds. Herein, the finally higher design tip speed and, thus, smaller chord are a result of the utilized material scaling boundary conditions (Schütt et al., 2020, 2021). However, adapting all layer thicknesses at a local position with only one factor might provide a very similar but not optimal layer stack. Increasing, e.g., the core material over-proportionally in the buckling-prone regions would presumably enable a sufficient structural stability for the blades of a two-bladed counterpart with wider chords and lower tip speeds. It would result in stiffer and lighter, ultra-size-ready blades with even more tip-to-tower clearance and less weight-induced edgewise fatigue loads, which will most likely become an increasingly important design driver for larger turbines. With such an approach, a two-bladed turbine could fully exploit its structural potential, which has been hindered herein due to the chosen boundary conditions. The use of less stiff and less strong, but better recyclable materials could also be an option for the naturally stiffer and lighter large chord designs of a two-bladed turbine and might also be an interesting future research topic. Furthermore, it is debatable whether it is mandatory for fair comparability that the blades of the two-bladed counterpart need to be superior regarding both the static and fatigue material stresses at all positions along the blades or if it is sufficient to maintain only the same maximal static and fatigue stress limits for the respective loads to avoid vast over-engineering. In that sense, the two-bladed turbine's blade scaled by analytical static loads in Section 2.2 might be a better compromise. It possesses a more transparent but still reasonable analytical load assumption (Anstock and Schorbach, 2021) and furthermore possesses a very similar maximum fatigue damage value for the standard fatigue design load case DLC 1.2 (see Figure 6 (b)).

2. The tower and the jacket foundation have been designed specifically for the needs of a three-bladed turbine. It did unintentionally place the first tower eigenfrequencies poorly for a similar two-bladed turbine. Since it has been unclear if the eigenfrequency placement, the stability, or the fatigue resistance had been the actual design driver, the latter has been

conservatively regarded as valid. A throughout tower and jacket design, possibly with a higher lattice structure, might
enable a higher tower eigenfrequency placement above the 2P-excitation that is more suitable for a two-bladed turbine
and potentially non-optimal for the 3P-excitation of a three-bladed turbine, a characteristic that can partially be observed
for very large floating turbines Anstock et al. (2023). Apart from that, the jacket foundation could also be replaced by
a more common monopile structure, while the tower design could be limited by a more conservative diameter of, e.g.,
10 m, like the IEA 22 MW reference wind turbine (Zahle et al., 2019), which would be easier to manufacture than the
11 m tower diameter herein. Both steps would reduce the first natural frequencies and push it towards 1P or even beyond.
Such a tower could solve the tower eigenfrequency issue of the two-bladed turbine (Anstock and Schorbach, 2021) and
could enable a more fair (tower) load comparability and render the tower dampers less mandatory, especially for the
two-bladed turbine.

Table 4. Summary of the main turbine characteristics.

	20 MW three-bladed reference[1]	20 MW two-bladed counterpart	20 MW two-bladed teeter-hub
Rotor diameter	252.2 m	257.4 m	257.4 m
Rotor orientation	upwind	upwind	upwind
Rated tip speed	90 m/s	101 m/s	101 m/s
Rated wind speed	11.4 m/s	11.4 m/s	11.4 m/s
Rated rotor speed	6.82 rpm	7.49 rpm	7.49 rpm
Controller concept	variable speed PI-controller (speed excl. zone & active tower dampers)	variable speed PI-controller (speed excl. zone & active tower dampers)	variable speed PI-controller (speed excl. zone & active tower dampers)
Blade mass	117.9 t	164.4 t (or 155.2 t)[2]	138.3 t
Total blade mass	353.7 t	328.8 t (or 310.4 t)[2]	276.6 t
Rotor mass (incl. hub)	636.2 t	611.2 t (or 592.9 t)[2]	559.1 t
Hub height	167.9 m	167.9 m	167.9 m
Tower height	163.14 m	163.14 m	163.14 m
Tower mass	1356.6 t	1826.0 t	1374.2 t
1st tower eigenfrequency	0.166 Hz	0.168 Hz	0.169 Hz
Drive train concept	direct drive	direct drive	direct drive
Nacelle mass	1098.0 t	1050.2 t	1050.2 t

[1] INNWIND 20 MW offshore reference wind turbine (Chaviaropoulos and Milidis, 2017; Sartori, 2019) with
retuned and extended controller (Anstock and Schorbach, 2020, 2021) and direct drive concept (see Section 5)
[2] Less over-engineered two-bladed counterpart that is designed for equal stability limits and similar static
material stresses along the blades, but only feature the same maximum blade fatigue damage (see Section 2.4).

3. The two-bladed turbine's dynamics are more challenging. Nonetheless, rather standard single-in-single-out proportional-(integral)-gain control concepts have been utilized herein to achieve objectivity for controller design and tuning (Anstock and Schorbach, 2020). Advanced, e.g. model-based predictive control methods might further close the gap between tower loads of two- and three-bladed turbines. Alternatively, there might be more suitable two-bladed control concepts, e.g. by "mimicking" the teeter excursion of about 3° with its amplitude's peak due to gyroscopic effects counter-intuitively in the vertical (Hohenemser and Swift, 1984) by enabling flexibility in the yaw system as proposed by van Solingen et al. (2016). In general, every research on load reduction for large two-bladed turbines would secure the knowledge of whether or not their largest drawback of more harmful dynamics is actually (un)avoidable.

Despite these critical and extensional thoughts, the proposed redesign methodology and the redesigned two-bladed 20 MW turbines do serve as a solid basis for further analyses and comparisons. They form the main outcome of the research project "X-Rotor – two-bladed wind turbines". Table 4 summarizes the main turbine characteristics of the 20 MW three-bladed reference, the 20 MW two-bladed counterpart, and the 20 MW two-bladed teeter-hub turbine. The turbine data, including the two- and three-bladed 20 MW aero-servo-elastic turbine models, the structural blade model, and the controller is made available online for scientists who are interested in further details or who would like to use these models for further analyses. The corresponding link is listed below within the section "code and data availability".

8 Conclusions

In the presented work, a most similar 20 MW two-bladed counterpart has been redesigned on the basis of the three-bladed 20 MW INNWIND reference wind turbine. It features similar aerodynamics by utilizing the same airfoils in the same relative positions, the same local angles of attack, and the same relative chord length layout. The blade stability margin matches the value of the three-bladed turbine. Regarding the blade material stresses, two design options are presented: one possesses equal static stresses along the blade, while the other has added material to reach equal fatigue damages along the blade. The former is, however, less over-engineered, it is based on a more transparent analytical load assumption, and still fulfills the demand of an equal fatigue lifetime by showing a similar maximum fatigue damage value. For the lower blade loads of a two-bladed turbine with a teetering hub, another structural blade design has been added. Finally, all controllers are equipped with the same control features, while the gains are tuned by an objective control cost criterion. The tower and the jacket foundation are left unchanged for the sake of consistency with the three-bladed reference turbine, resulting in higher tower loads, masses, and costs if no load mitigation concept, such as a teetering hub, is used. Note that a monopile foundation and a more slender tower would have been beneficial for the two-bladed turbine due to their naturally lower eigenfrequency, which better suits their blade-passing excitation frequency. The drive train has been transformed into a direct drive for the reference turbine and scaled down for the faster rotation speed of the two-bladed turbine. Finally, the two-bladed turbine's rotor radius is slightly extended by 2 %, to achieve on equal absolute power curve compared to the three-bladed turbine. This most comparable design enables to contrast loads, dynamics and costs of the 20 MW two-bladed and three-bladed turbines directly, without scaling the results to another energy yield. The turbine models are made accessible open source with the paper at hand.

In addition to the presented turbines, this manuscript showcases the methodology's redesign steps to inspire other researchers to perform a similar redesign and gain their own two-bladed turbine based on their own three-bladed reference. It is the authors' aim to highlight also the weak sections of the proposed redesign approached to support similar attempts with valuable lessons learned. Concluding it can be stated that a sufficient utilization of the structural benefits from a wider blade chord, along with a sophisticated active or passive load mitigation concept, and a suitable first eigenfrequency of the tower and (monopile) foundation might be key elements for the success of large offshore two-bladed wind turbines in the future.

Finally, the authors must acknowledge that a comparison between two- and three-bladed turbines is indeed notoriously difficult, as already mentioned by Burton et al. (2021). Nevertheless, consistent and strict assumptions must be made when conducting a comparison between such technically complex systems. Using the concept of "fair comparibility", which has, in retrospect, been rather disadvantageous for the two-bladed turbine, somehow draws attention to the unique characteristics of two-bladed turbines. In the end, it is this uniqueness that offers completely new concepts for further load reductions and lets the authors come to the conclusion that further research on two-bladed turbines is still important. Hopefully, the presented findings and published data can serve as a basis and invite scientists and companies to do further research on two-bladed turbines to gain answers on whether large two-bladed or still three-bladed turbines are the more economical concept for future offshore wind installations.

Code and data availability. The controller, the aero-servo-elastic two- and three-bladed 20 MW wind turbine models in the software DNV® Bladed, as well as the structural blade model in the software NuMAD are published open access on GitHub. Please follow https://github.com/X-Rotor/two-bladed-wind-turbines or the DOI 10.5281/zenodo.13269498 to the respective files.

Author contributions. Fabian Anstock designed and programmed the controller, including all its additional features. He performed most aeroelastic load analyses, re-designed the aerodynamic surface of the blades, made the analytical blade and tower structure changes, and wrote this paper primarily. Marcel Schütt performed all finite element and fatigue analyses concerning the structural blade design. This includes the generation of detailed structural blade models. Vera Schorbach guided the research and assisted with valuable feedback, ideas, and technical advice.

Competing interests. The authors declare that they have no conflict of interest.

Acknowledgements. The present work is part of the four-year research project "X-Rotor – two-bladed wind turbines" funded by the German Federal Ministry of Education and Research and Siemens Gamesa Renewable Energy (reference 13FH1I04IA), whom we would here like to thank. This paper is funded by the Publication-Fonds of the Hamburg University of Applied Sciences.

References

425   Aagaard Madsen, H., Bergami, L., and Rasmussen, F.: New aerodynamics rotor concepts specifically for very large offshore wind turbines, INNWIND Deliverables, 2.11, 1–78, 2013.

Anderson, M. B., Garrad, A. D., and Hassan, U.: Teeter excursions of a two-bladed horizontal-axis wind-turbine rotor in a turbulent velocity field, Journal of wind engineering and industrial aerodynamics, 17, 71–88, https://doi.org/https://doi.org/10.1016/0167-6105(84)90035-7, 1984.

430   Anstock, F. and Schorbach, V.: A control cost criterion for controller tuning of two- and three-bladed 20 MW offshore wind turbines, Journal of Physics: Conference Series, 1618, 022 062, https://doi.org/https://doi.org/10.1088/1742-6596/1618/2/022062, 2020.

Anstock, F. and Schorbach, V.: The effect of a speed exclusion zone and active tower dampers on an upwind fixed-hub two-bladed 20 MW wind turbine, Journal of Physics: Conference Series, 2018, 012 003, https://doi.org/10.1088/1742-6596/2018/1/012003, 2021.

Anstock, F. and Schorbach, V.: The Effect of Rotor Size on the Teeter Behavior of Two-Bladed Wind Turbines, Renewable Energy
435   [Manuscript submitted for publication. Preprint available at SSRN: http://dx.doi.org/10.2139/ssrn.4968596], 2024.

Anstock, F., Schütt, M., and Schorbach, V.: A new approach for comparability of two- and three-bladed 20 MW offshore wind turbines, Journal of Physics: Conference Series, 1356, 012 008, https://doi.org/10.1088/1742-6596/1356/1/012008, 2019.

Anstock, F., Kessler, A., and Schorbach, V.: Increased tower eigenfrequencies on floating foundations and their implications for large two- and three-bladed turbines, J. Phys.: Conf. Ser., 2626, 012 002, https://doi.org/10.1088/1742-6596/2626/1/012002, 2023.

440   Blasques, J. P. and Stolpe, M.: Multi-material topology optimization of laminated composite beam cross sections, Composite Structures, 94, 3278–3289, https://doi.org/https://doi.org/10.1016/j.compstruct.2012.05.002, 2012.

Blevins, R. D.: Formulas for dynamics, acoustics and vibration, John Wiley & Sons, https://doi.org/https://doi.org/10.1002/9781119038122, 2015.

Burton, T., Jenkins, N., Bossanyi, E., Sharpe, D., and Graham, M.: Wind Energy Handbook, Wiley, 3rd edn., ISBN 978-1-119-45109-9,
445   2021.

Chaviaropoulos, P. K. and Milidis, A.: 20 MW Reference Wind Turbine, INNWIND Deliverables 1.25 (a), 2017.

Civati, M., Sartori, L., and Croce, A.: Design of a two-bladed 10 MW rotor with teetering hub, Journal of Physics: Conference Series, 1037, 042 007, https://doi.org/10.1088/1742-6596/1037/4/042007, 2018.

Gaertner, E., Rinker, J., Sethuraman, L., Zahle, F., Anderson, B., Barter, G., Abbas, N., Meng, F., Bortolotti, P., Skrzypinski, W., Scott, G.,
450   Feil, R., Bredmose, H., Dykes, K., Shields, M., Allen, C., and Viselli, A.: Definition of the IEA 15-Megawatt Offshore Reference Wind Turbine, Tech. Rep. NREL/TP-5000-75698, National Renewable Energy Laboratory, 2020.

Hansen, M. H. and Henriksen, L. C.: Controller description Land Version (Basic DTU Wind Energy Controller), INNWIND Deliverable 1.21, 2013.

Henderson, G. M., Haines, R. S., and Quarton, D.: The Analysis and Design Implications of Pitch-Teeter Coupling, EWEC, 1989.

455   Hohenemser, K. H. and Swift, A.: On the Design of Horizontal axis two Bladed Hinged Wind Turbines, Journal of Solar Energy Engineering, 1984.

Jamieson, P.: Innovation in Wind Turbine Design, John Wiley & Sons, 2nd edn., ISBN 978-1-119-13790-0, 2018.

Larsen, T. J., Aagaard Madsen, H., Thomsen, K., and Rasmussen, F.: Reduction of teeter angle excursions for a two-bladed downwind rotor using cyclic pitch control, Proceedings of EWEA, 2007.

460 McCoy, A., Musial, W., Hammond, R., Hernando, D. M., Duffy, P., Beiter, P., Pérez, P., Baranowski, R., Reber, G., and Spitsen, P.: Offshore Wind Market Report: 2024 Edition, NREL/TP-5000-90525. https://www.nrel.gov/docs/fy24osti/90525.pdf, 2024.

Mühle, F., Adaramola, M. S., and Sretran, L.: The effect of the number of blades on wind turbine wake - A comparison between 2- and 3-bladed rotors, Journal of Physics: Conference Series, 753, 032 017, https://doi.org/10.1088/1742-6596/753/3/032017, 2016.

Prandtl, L.: Applications of modern hydrodynamics to aeronautics, National Advisory Committee for Aeronautics, 116, 1923.

465 Sartori, L.: System Design Of Lightweight Wind Turbine Rotors, Ph.D. thesis, Politecnico Milano, 2019.

Schorbach, V.: Pendelendanschläge bei Zweiblatt-Windenergieanalgen, Ph.d., University of Wuppertal, https://doi.org/10.51202/9783186433015, 2016.

Schorbach, V., Dalhoff, P., and Gust, P.: Teeter design for lowest extreme loads during end impacts, Wind Energy, 21, 1–14, https://doi.org/10.1002/we.2140, 2017.

470 Schütt, M., Anstock, F., and Schorbach, V.: Progressive structural scaling of a 20 MW two-bladed offshore wind turbine rotor blade examined by finite element analyses, Journal of Physics: Conference Series, 1618, 052 017, https://doi.org/10.1088/1742-6596/1618/5/052017, 2020.

Schütt, M., Anstock, F., and Schorbach, V.: A procedure to redesign a comparable blade structure of a two-bladed turbine based on a three-bladed reference, Journal of Physics: Conference Series, 2018, 012 035, https://doi.org/10.1088/1742-6596/2018/1/012035, 2021.

Shrestha, G., Polinder, H., and Ferreira, J. A.: Scaling laws for direct drive generators in wind turbines, 2009 IEEE International Electric Machines and Drives Conference, pp. 797–803, https://doi.org/10.1109/IEMDC.2009.5075295, 2009.

475 van Solingen, E., Beerens, J., Mulders, S. P., De Breuker, R., and van Wingerden, J. W.: Control design for a two-bladed downwind teeterless damped free-yaw wind turbine, Mechatronics, 36, 77–96, https://doi.org/https://doi.org/10.1016/j.mechatronics.2016.03.008, 2016.

Zahle, F., Barlas, A., Lønbæk, K., Bortolotti, P., Zalkind, D., Wang, L., Labuschagne, C., Sethuraman, L., and Barter, G.: Definition of the IEA Wind 22-Megawatt Offshore Reference Wind Turbine, Technical University of Denmark, 4, 68, https://doi.org/10.11581/DTU.00000317,
480 2019.